Nitriding and Nitrocarburizing; Current Status and Future Challenges

Somers, Marcel A. J.

Publication date:
2013

Document Version
Peer reviewed version

Nitriding and Nitrocarburizing: Status and Future Challenges

Marcel A.J. Somers

Technical University of Denmark, Dept. of Mechanical Engineering, 2800 Kgs. Lyngby, Denmark
somers@mek.dtu.dk

Keywords: Nitriding, nitrocarburizing, microstructure evolution, compound layer, diffusion zone, expanded austenite

Abstract. This contribution addresses the current understanding of gaseous nitriding and nitrocarburizing. Aspects of thermodynamics, kinetics and microstructure development in iron and heat treatable steel will be explained. In these materials the nitrided/ nitrocarburized case can be subdivided in a compound layer consisting of iron (carbo-)nitrides and a diffusion zone, consisting of a dispersion of alloying element nitrides in ferrite. The compound layer provides beneficial tribological and corrosion performance, while the diffusion zone is responsible for improved fatigue performance. Furthermore, aspects of low temperature surface hardening of stainless steels in a gaseous environment will be addressed. Here, the developed case consists of expanded austenite and/or expanded martensite, which essentially is a super saturated solid solution of nitrogen/carbon in austenite/martensite. The current state of the art and necessary future research activities for improvement of the present understanding will be identified.

Introduction

Gaseous thermochemical surface treatments as nitriding and nitrocarburizing belong to the most versatile surface engineering processes of steels and allow improvement of the performance of components with respect to fatigue, wear and atmospheric corrosion. The case developing during treatment can be subdivided in a compound layer at the surface and a diffusion zone underneath. The compound layer consists of iron (carbon)nitrides γ'-Fe_4N_{1-x} and ε-$Fe_2(N,C)_{1-z}$, while the diffusion zone consists of alloying element (carbo)nitrides (e.g. CrN and AlN) or a supersaturated interstitial solution of nitrogen in a metallic matrix. The compound layer provides wear resistance and, particularly after post-oxidation, enhanced performance with respect to atmospheric corrosion. The diffusion zone is responsible for dramatic improvement of fatigue performance, by evoking a compositionally induced compressive residual stress profile. In contrast with case hardening by carburizing the surface hardening effect obtained by nitriding/ nitrocarburizing is not achieved by a martensitic transformation in the material.

Classical *nitriding* is performed in the temperature range 480-530 °C for 20-80 h and the main purpose is the development of a diffusion zone to enhance the fatigue performance of a component. *Nitrocarburizing* is performed at 540-590 °C and has the development of a compound layer with good wear and tribological performance as the main objective. This manuscript conveys the fundamentals of the influence of incorporating nitrogen, during gaseous nitriding, and nitrogen and carbon, during gaseous nitrocarburizing, on the microstructure of the developing case. The basic mechanisms of microstructure formation revealed by such gaseous treatment are transferable to salt-bath and plasma treatments.

Thermodynamic principles of nitriding and nitrocarburizing

For gaseous nitriding in NH_3/H_2, adsorbed nitrogen atoms can diffuse into the solid phase ϕ [1,2]:

$$NH_3 \rightleftarrows N_{ad} + \tfrac{3}{2} H_2 \qquad \text{(Ia)}$$

$$N_{ad} \rightleftarrows [N]_{\phi} \qquad \text{(Ib)}$$

or leave the surface again: $N_{ad} + N_{ad} \rightleftarrows N_2$ (Ic)

In principle, reaction (Ic) is thermodynamically preferred over reaction (Ib), but nitriding according to reaction (Ib) is possible is possible due to limited kinetics of (Ic). For temperatures below 460 °C, reaction (Ic) can practically be neglected.
For nitrocarburizing, the important carburizing reactions in the presence of hydrogen, are [3]:

$CO_2 + H_2 \rightleftarrows CO + H_2O$ (IIa)

$CO + H_2 \rightleftarrows C_{ad} + H_2O$ (IIb)

$C_{ad} \rightleftarrows [C]_\phi$ (IIc)

In principle carburizing could also proceed according to:

$2CO \rightleftarrows C_{ad} + CO_2$ (IId)

followed by reaction (IIc), but reaction (IId) proceeds much slower than reaction (IIb).
Additionally, the following reactions can occur [1]:

$CO + NH_3 \rightleftarrows HCN + H_2O$ (IIIa)

$HCN \rightleftarrows N_{ad} + C_{ad} + \frac{1}{2} H_2$ (IIIb)

which are promoted by the presence of catalytic surfaces in the furnace, as for example the furnace lining or fixtures. On the basis of reactions (Ia) and (IIb) the activities of adsorbed nitrogen, a_N, and carbon, a_C, can be defined at 1 bar pressure:

$$a_N = K_{Ia} \cdot K_N \qquad K_N = p_{NH_3} \big/ p_{H_2}^{3/2}$$
$$a_C = K_{IIb} \cdot K_C \qquad K_C = p_{CO}\, p_{H_2} \big/ p_{H_2O} \qquad \text{(IV)}$$

where K_{Ia} and K_{IIb} are the temperature dependent equilibrium constants of reactions (Ia) and (IIb), respectively, and K_N and K_C are nitriding potential and carburizing potential, respectively. Only for the case that the gas phase reaction (IIa) is in equilibrium are the carbon activities imposed by reactions (IIb) and (IId) equal. Although this is often assumed [4], this is generally not the case [5].

The stability of the various iron-based nitrides is depicted in the so-called Lehrer diagram (Fig.1) [6].
The stability ranges of the iron nitrides follow from the Fe-N phase diagram (Fig.2), which shows that γ'-Fe_4N_{1-x} has a narrow homogeneity range, comparable in width to ferrite. This narrow homogeneity range corresponds to a broad composition range in the gas mixture (see the Lehrer diagram in Fig.1). The ε-Fe_2N_{1-z} phase has a broad homogeneity range and, for temperatures below 592 °C, is first stabilized at nitrogen contents beyond those necessary to stabilize γ'-Fe_4N_{1-x}. The composition of the Fe-N phases can be accurately controlled by adjusting the nitriding potential K_N, as depicted in so-called absorption isotherms [7-9]. These compositions would in principle be expected at the surface of a growing compound layer.
Systematic studies on the Fe-N-C system were published as phase stability diagrams for iron powder nitrocarburized in flowing NH_3-H_2-CO gas mixtures (Fig. 3) [10] and isothermal sections of the iron rich corner of the ternary Fe-N-C phase diagram (Fig.4) [11]. Unfortunately, as the water vapour content (pH_2O) in the applied gas mixtures was not provided, the carbon activity in the phase diagram was uncontrolled (see Eq. (IIb)). This hinders a straightforward thermodynamic approach of the available data. Figs. 3 and 4 show that the presence of a carbon containing gas in the nitrocarburizing atmosphere stabilizes the ε-phase and suppresses the development of the γ'-phase.

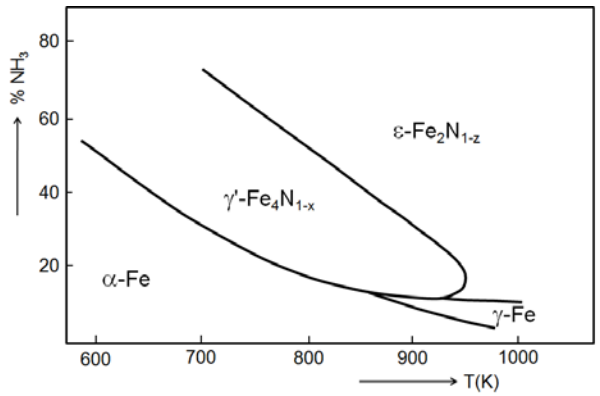

Fig.1: Stability of Fe-N phases; Lehrer diagram [6].

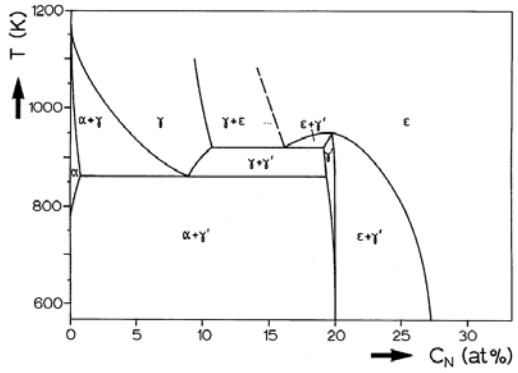

Fig.2: Fe-N phase diagram.

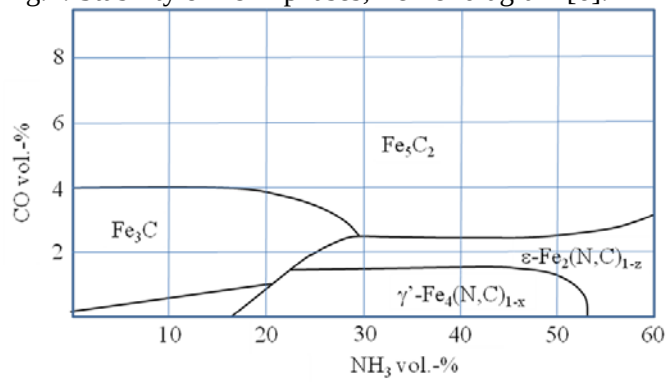

Fig.3: Phase stability of Fe-N-C phases at 500 °C in NH_3-CO-H_2 gas mixtures [10].

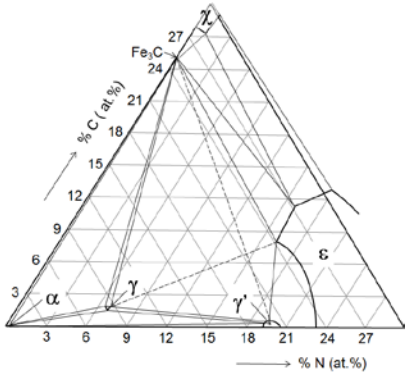

Fig.4: Isothermal section of the Fe-N-C phase diagram at 570°C (843 K) [11].

Kinetics of compound layer formation

The development of the compound layer during nitriding proceeds along the stages depicted in Fig. 5 [12]. Thermodynamically, the first phase developing at the surface of iron on gaseous nitriding, is γ'-Fe_4N_{1-x}. The incubation time for the nucleation of γ' nitride depends on the actual nitrogen content at the surface, which is the net effect of a competition between the fluxes of nitrogen atoms arriving at the surface and the fluxes of nitrogen atoms leaving the surface (Fig.7) [9,13]. The flux of arriving nitrogen atoms is controlled by the dissociation rate of ammonia (reaction (Ia)); the fluxes of leaving nitrogen atoms are those diffusing into the solid state (reaction (Ib)) and desorbing as N_2 (reaction (Ic)). After the nucleation of γ' nitride ε-phase can nucleate on top (Fig.5b). Coalescence of dual phase nuclei establishes a ε/γ'-bi-layer, which grows under the influence of nitrogen diffusion through the layer (Fig. 5c). In this stage both γ' and ε layers grow parabolically with time [14].

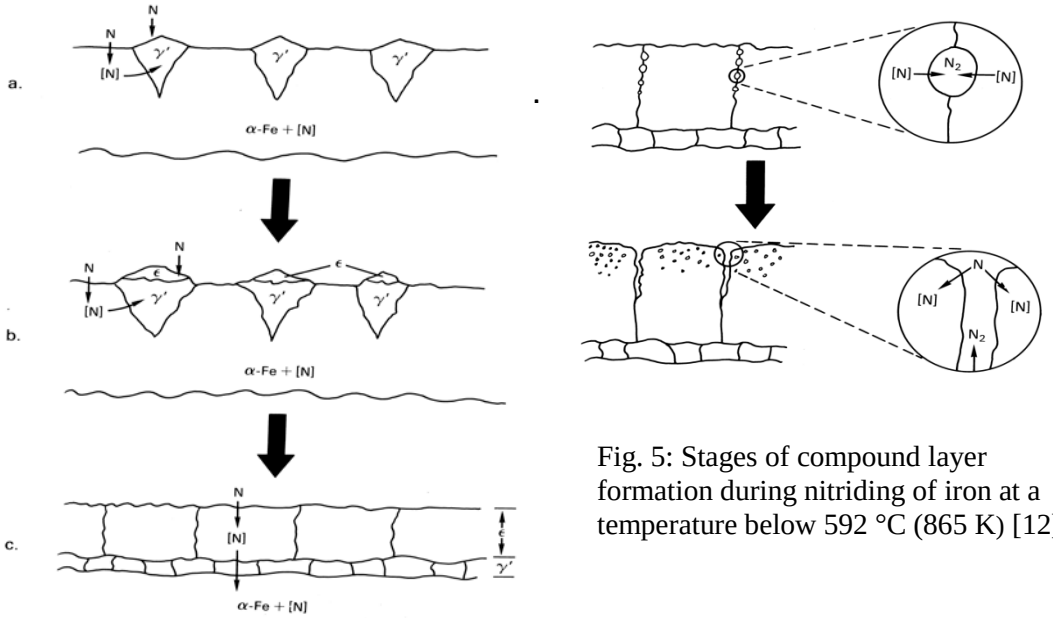

Fig. 5: Stages of compound layer formation during nitriding of iron at a temperature below 592 °C (865 K) [12].

The thickness ratio of the ε and γ' layers in the compound layer depends on the nitriding parameters temperature and nitriding potential. In principle the thickness ratio should be time independent, provided that coupled growth of the ε and γ' layers is strictly diffusion controlled. The effect of the nitriding potential is illustrated in Fig. 7 [14]. As a consequence of the inherent metastability of iron nitrides at 1 bar with respect to Fe and N_2 (see above) porosity develops in the compound layer on prolonged nitriding. The associated development of N_2 is firstly observed at energetically favourable nucleation sites in the region with the highest nitrogen content, i.e. near the surface at grain boundaries, where the highest driving force for N_2 development occurs (Fig. 5d). On continued nitriding (or during ageing) the pores coalesce and form pore channels, which allow the gas mixture to reach the interior of the porous nitride layer (Fig. 5e).

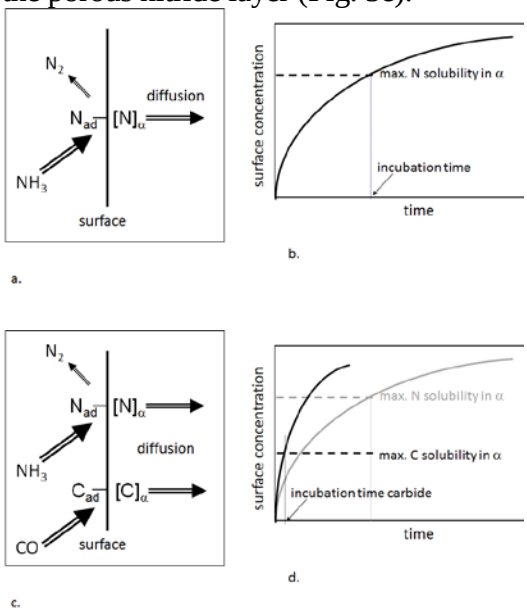

Fig.6: Flux balance at iron surface during nitriding (a.) and nitrocarburizing (c.) leads to gradual increase of the surface concentration of nitrogen/carbon and incubation time for nucleation (b./d.) [13].

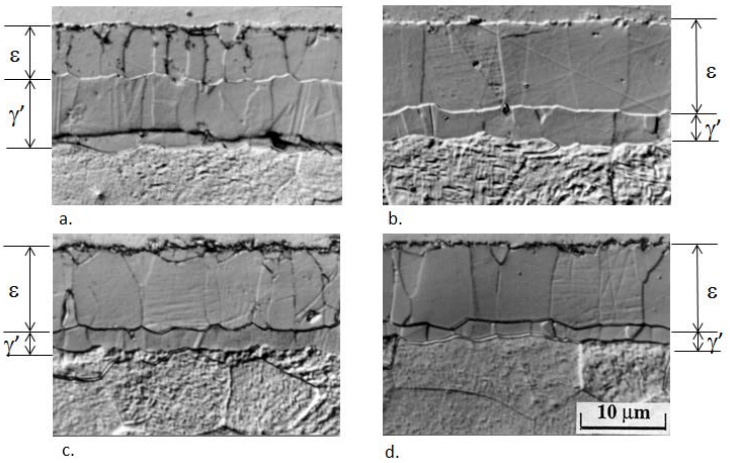

a. K_N=2, t=10 h; b. K_N=4, t=6 h;

c. K_N=6, t=3 h; d. K_N=8 t=3 h;

Fig.7: ε/γ' double layers on pure iron obtained at 550 °C (823 K) for nitriding potential K_N and nitriding time, t [14].

On *nitrocarburizing* the nucleation of the phases at the surface depends on the competition of the surface reactions (I) and (II) (Fig.6c). The carburizing reaction (IIb) proceeds usually much faster than the nitriding reaction (Ib). Furthermore, ferrite has a lower solubility for carbon than for nitrogen. Hence, the maximum carbon content dissolvable in the substrate surface is exceeded earlier than the nitrogen solubility (Fig.6d) and an iron-carbide nucleates [15]. Nucleation of γ' iron nitride is suppressed (cf. Fig.3 and 4). The development of the composition and morphology of the compound layer is schematically shown in Fig.8 [12]. On nitrocarburizing pure iron the first phase appearing at the surface is cementite (θ-Fe_3C) [5]. The appearance of the iron-carbonitride phase ε-$Fe_2(N,C)_{1-z}$ (after cementite nucleation) in the compound layer is promoted by a high nitriding potential and is retarded by a high carburizing activity. So far, ε-phase has not been observed to nucleate as the first phase at the iron surface during nitrocarburizing.

After the initial development of cementite, the ε-phase becomes dominant in the compound layer on prolonged treatment. The content of cementite decreases and, eventually, cementite disappears, provided that the carburizing potential is lower than that necessary to stabilize cementite. Concurrently, the amount of γ' phase increases (see Fig. 8b), particularly in the part of the compound layer adjacent to the substrate along with a redistribution of the carbon initially incorporated. Due to the relatively slow kinetics of ammonia dissociation at the iron surface and the concurrent nitrogen desorption, which initially allow a strong absorption of carbon, the composition of the compound layer evolves such that the nitrogen content at the surface increases gradually with time, while the corresponding carbon

content decreases complementarily [5,13]. Eventually, analogous to nitriding, a continuous γ'-layer underneath the ε-layer can develop, provided that the initially incorporated carbon is redistributed and does not hinder its development.

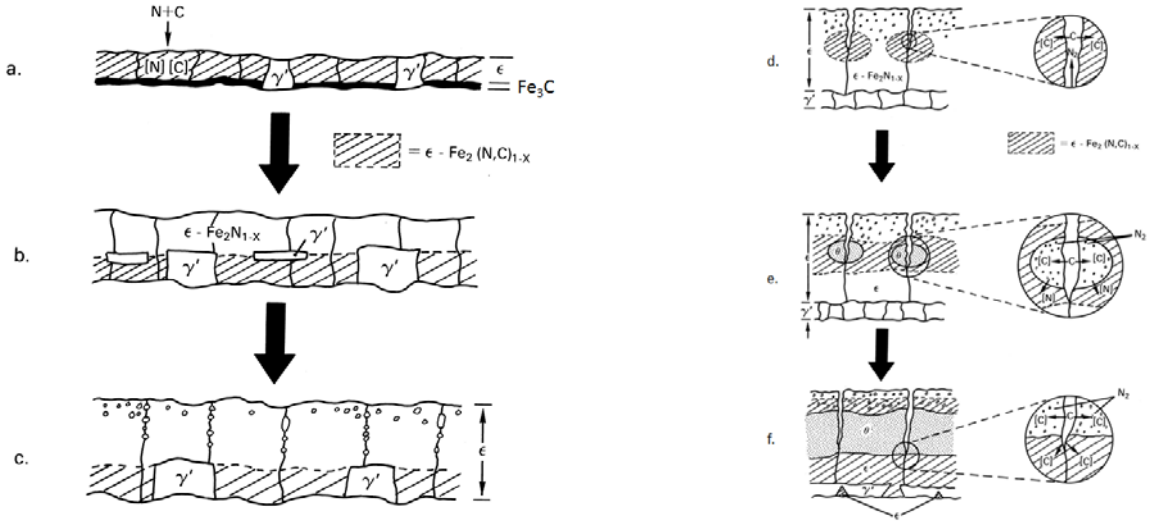

Fig.8: Stages of compound layer development during nitrocarburizing of iron at a temperature below 592°C (865 K) [12].

Upon the development of porosity in the compound layer, an additional mechanism for the incorporation of carbon into the compound layer from the nitrocarburizing atmosphere becomes possible (Fig.8d [15]): the uptake of carbon in the porous part of the compound layer at some distance from the surface. Prolonged incorporation of carbon in the porous part leads to the formation of cementite, firstly along the pore channels (Fig. 8e) and later as intermediate layer (Fig.8f).
A few examples of compound layers developing during nitrocarburizing are shown in Fig.9 [14]. The effect of a (too) high carburizing potential is clearly observed from comparing the compound layers in Figs. 9a and 9b. The only difference between the process conditions is a partial replacement of half the volume of CO by CO_2. In a CO containing gas mixture a higher carburizing potential can be achieved on nitrocarburizing than in a gas containing only CO_2. Consequently, Hägg carbide and cementite (cf. Fig.4) developed in the compound layer in Fig.9a and hinder fast growth of the compound layer, because these carbide phases can dissolve only small amounts of nitrogen and act as a diffusion barrier.

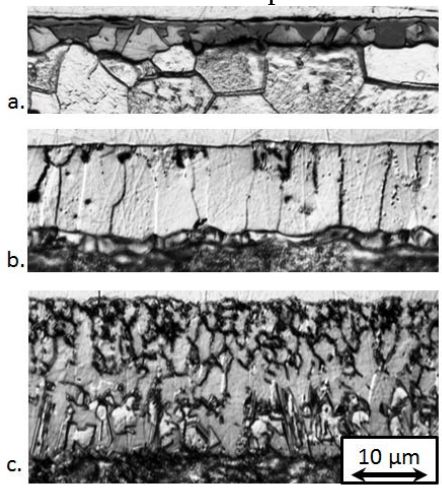

Fig.9: Compound layers obtained after nitrocarburizing at T=570 °C (843 K) for t=3 h.
a. Fe: 55% NH_3- 35 % H_2- 10 %CO;
b. Fe: 55% NH_3- 35 % H_2-5 %CO_2- 5 %CO;
c. Fe-0.4 C: 55% NH_3- 35 % H_2-5 %CO_2- 5 %CO [14].

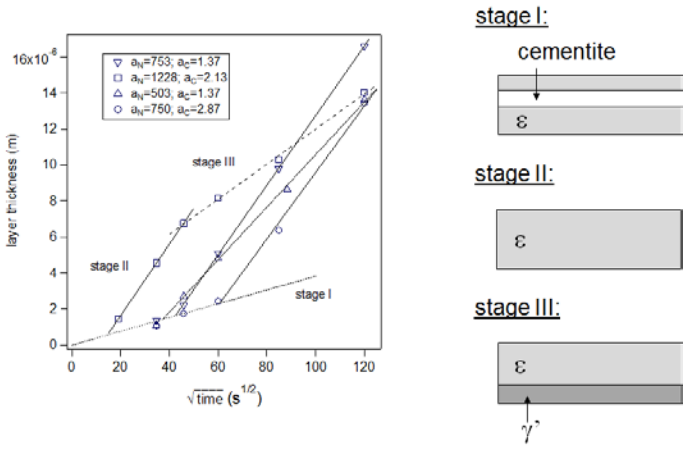

Fig.10: Kinetics of compound layer growth during nitrocarburizing of iron can be subdivided in 3 stages (I,II,III). Data points are for various combinations of nitrogen activity (a_N) and carbon activity (a_C) in the gas phase [5,13].

Replacing part of the CO with CO_2 a relatively thick, carbon lean, ε/γ' double layer develops, showing the onset of porosity close to the surface. The supply of carbon from the substrate for nitrocarburizing conditions as in Fig.9b follows from Fig.9c, where a thick, almost monophase ε-carbonitride, compound layer is shown with only a small amount of γ'-nitride and abundant porosity.
As suggested by Fig.9, the composition of the compound layer developing during nitrocarburizing, has a large influence on the growth kinetics. Comparison of compound layers grown for different combinations of nitrogen activity (a_N) and carbon activity (a_C) has revealed that essentially three stages of growth can be distinguished (Fig.10) [5,13]. Stages I and III are characterised by relatively slow layer growth kinetics, while stage II represents relatively fast layer growth kinetics. The transition from stage I to stage II coincides with a change of the dominant phase in the compound layer from cementite (and/or Hägg carbide) to ε-phase. The transition from stage II to stage III is associated with the appearance of a γ'-layer in-between the ε-phase and the underlying ferrite. Isolating the ε-phase from direct contact with the substrate by the appearance of γ'-nitride retards layer growth kinetics (cf. Fig.9b). If carbon is provided by the substrate the development of γ'-nitride in-between ε-carbonitride and the substrate can be prevented (Fig.9c). Accordingly a stage II to stage III transition of layer-growth kinetics does not occur.

Nitriding of steels

In the previous chapter the development of a diffusion zone underneath the compound layer was omitted. As long as no nitride-forming alloying elements are present, the diffusion zone at the nitriding temperature is essentially a solution of nitrogen in ferrite. For other steels a different picture emerges. Below the nitriding of heat treatable steel containing nitride forming elements and the nitriding/ nitrocarburizing of stainless steels, an emerging application, are discussed.

In steels containing alloying elements as for example Cr, Al, Mo, V and Ti, which are stronger nitride formers than iron, nitrides of type M_mN_n (M=Cr,Al,Mo,V, Ti) develop preferentially. Extensive investigations have been done on the nitriding of binary Fe-M alloys [e.g. 16-26] and some ternary iron-based alloys [e.g. 27-29]. From these investigations the picture emerges that if these nitride-forming alloying elements are in solid solution in the matrix, a dispersion of nano-scale platelike nitrides forms in the matrix for the nitrides with a NaCl type lattice (CrN, TiN, VN) and a hard diffusion zone develops. The growth of the diffusion zone is rate-controlled by the diffusion of nitrogen in the ferrite matrix [20, 30-33]. The capacity for binding nitrogen in the diffusion zone increases with the alloying element content. Generally, it is observed that the higher the content of strong nitride forming elements in ferrite, and, hence, the larger the capacity for binding nitrogen in the diffusion zone, the slower does the diffusion zone grow. If a compound layer has developed at the surface, the compound layer is the thinner the higher is the concentration of nitride-forming alloying elements in the diffusion zone.
On nitriding steels the carbides in the ferrite matrix are gradually transformed into (carbo-)nitrides. The carbon released by conversion of primary carbides develops cementite along grain boundaries lying within 45° inclined to the surface for strain energy minimization reasons (Fig.11). Ahead of the nitriding front carbon accumulates [34-36] and contributes to growth of primary carbides [35,36]. The grain boundary cementite can subsequently be transformed into carbon rich ε-phase and eventually grain boundary γ'-nitride [36].
The major contribution to materials performance improvement by the diffusion zone is provided by the development of dispersed alloying element nitrides. They are responsible for the hardness increase by precipitation hardening and induce the compressive residual stress profile as a consequence of the misfit with the matrix. For this reason it is important that a sufficient level of nitride-forming alloying elements is dissolved in ferrite. The growth of primary carbides ahead of the advancing nitriding front leads to a reduction of the concentration of dissolved nitride forming elements, and thus to a lower amount of alloying element nitrides at larger depth.

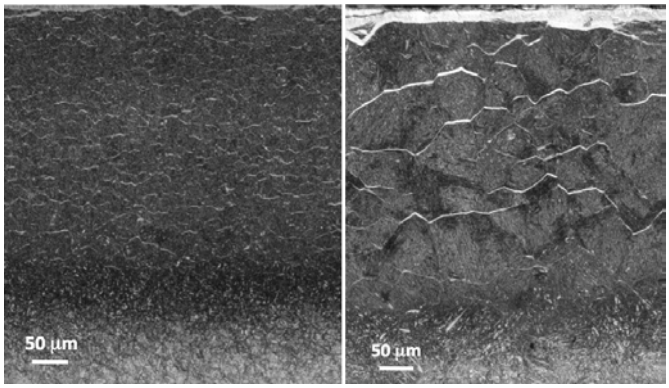

Fig.11: Cross sections of the diffusion zone in 33CrMoV12 9 nitrided at 520°C (793 K) for 100 h. The steels in have grain an average grain size of 15 µm (left) and 85 µm (reight). Network of (converted) carbides along grain boundaries develop [36].

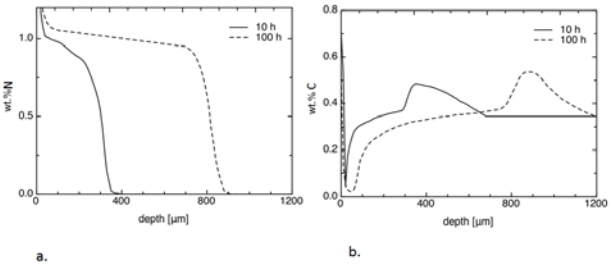

Fig.12: Composition depth profiles for nitrogen (a.) and carbon (b.) for a Fe-Cr-C alloy (3.0 wt% Cr, 0.35 wt% C) nitride at 550°C (823 K) for 10 and 100h. Profiles were determined with (GDOES) [35].

The effect of alloying element concentration, nitriding time and nitriding temperature on the stress distribution in the diffusion zone is summarized in Fig. 13 [37]. Stress build up is considered to be caused by nitride precipitation, while stress relaxation is a consequence of carbon depletion and overaging of the nitrides. Clearly, the higher the concentration of nitride-forming alloying elements, the higher is the compressive residual stress in the diffusion zone, the shallower is the diffusion zone and the steeper is the stress gradient at the case-core transition. For increasing nitriding time, the contribution of carbon depletion becomes more pronounced and the maximum in compressive residual stress is shifted to larger depth, while its magnitude decreases. Lastly, an increase of the nitriding temperature contributes to a deeper diffusion zone as growth proceeds faster, but also a lower maximum compressive residual stress, resulting from more carbon depletion and faster overaging [37].

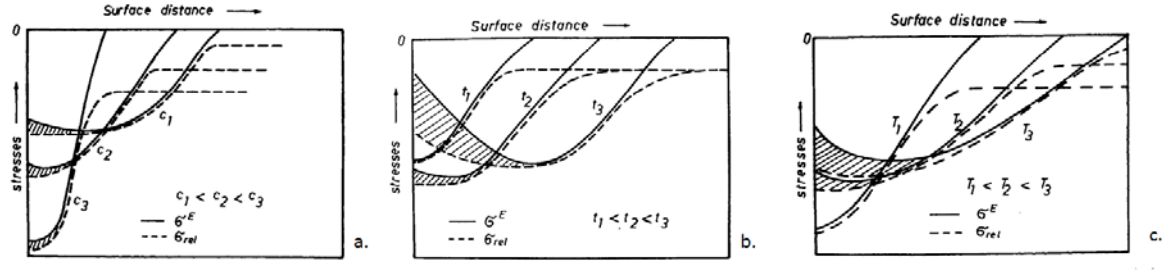

Fig. 13: Evolution of residual stress profiles in the diffusion zone with concentration of nitride formers, c (a), with nitriding time t (b), with nitriding temperature, T (c). The shaded areas mark stress relaxation as a consequence of decarburization and overaging (σ_{rel}=relaxation stress; σ_E=elastic stress due to volume mismatch) [37].

Generally, nitriding/nitrocarburizing of stainless steels in the conventional temperature range 490-580 °C is not considered good practice as such treatment will lead to the precipitation of CrN. Although this provides a hardening effect, the stainless character is lost, because free chromium is no longer available to maintain the passive layer. Since the mid-1980s several processes were developed that enable low temperature surface hardening of stainless steel at temperatures below 440 °C [38]. A schematic TTT diagram is given in Fig. 14 and demonstrates the allowable treatment time at low temperature before precipitation of Cr-nitrides occurs. In this temperature range nitrogen and carbon diffuse over a relatively long distance while substitutional alloying elements can be considered stationary. Consequently, the development of nitrides or carbides proceeds slow enough to establish a nitrogen or carbon rich case that is free of chromium-nitrides/carbides. These processes produce a case that is essentially a solid solution of high amounts of nitrogen (and/or carbon) in austenite, so-called expanded austenite, or in case of martensite, expanded martensite (see reviews in [39,40]). Initially plasma processes were employed, because

surface activation by removal of the passive film through sputtering is an inherent step in such treatments. In the latter years also gaseous treatments with in-situ surface activation have reached maturity [41-45]. Gaseous processes enable the largest flexibility and straightforward thermodynamic definition as regards process parameters, and are therefore treated exclusively. As an example austenitic stainless steel is described.

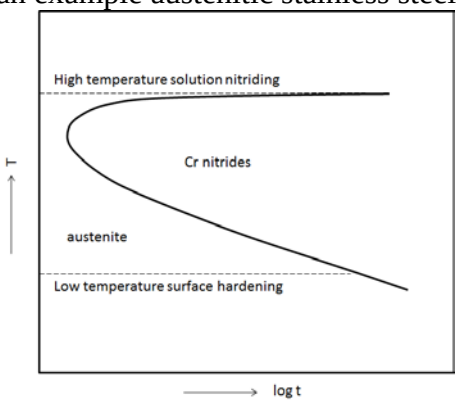

Fig. 14: Schematic TTT diagram of austenite with a high nitrogen content.

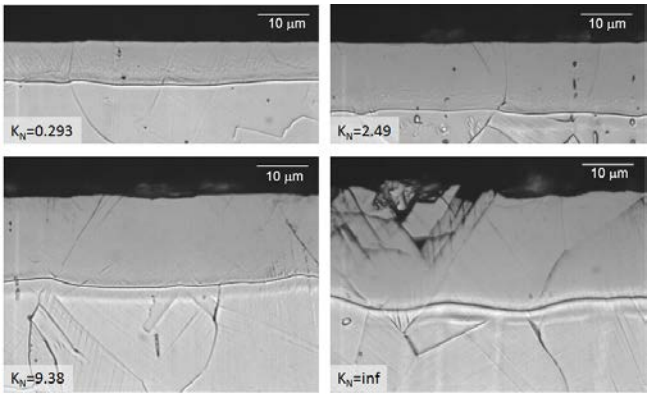

Fig.15: Cross sections of AISI 316 nitrided at 445 °C (718 K) for 22 h in NH_3-H_2-N_2 gas mixtures, at various nitriding potentials, K_N [41,46] .

Nitriding of austenitic stainless steel produces an almost featureless case at the surface (Fig. 15), indicating that this zone is more resistant against the etchant (aqua regia) than austenite. The transition from expanded austenite to austenite is not marked by an actual interface, but by a steep change in composition. A continuation of grain boundaries from austenite into the developed case proves that the case is merely a (supersaturated) solid solution in nitrogen and not a new phase. Therefore, the designation expanded austenite is more appropriate than S-phase. Nitriding at various nitriding potentials allows a variation of the composition range and depth range of expanded austenite [42,46]. Maximally, a colossal amount of up to 61 nitrogen atoms per 100 metal atoms (38 at.%N) can be dissolved in the developing case, corresponding Cr:N=1:3. Nitrogen solubilities in this composition range are far beyond the maximum solubility for nitrogen in iron austenite, which is about 10 at.% at T=650 °C (Fig.2). An explanation for the very high nitrogen solubility is the occurrence of short range ordering of chromium and nitrogen (or carbon) atoms, which leads to nitrogen occupation of octahedral interstices adjacent to chromium atoms. For the lowest nitrogen content in expanded austenite, i.e. for Cr:N=1:1, on average each Cr atom is coordinated by 3 neighboring N atoms [47].

The colossal increase in interstitial atom content in austenite leads to solid-solution strengthening and a spectacular increase in hardness. Examples of the increase in hardness in the nitrided (and carburized) case are shown in Fig.16.

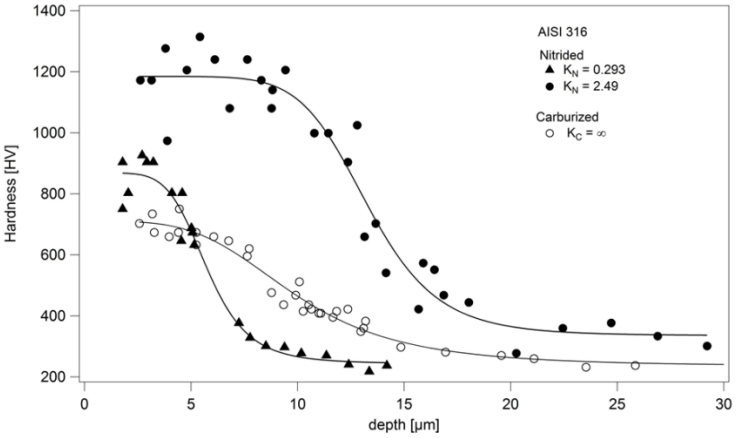

Fig.16: Hardness-depth profiles of AISI 316 nitrided at 445 °C (718 K) for 22 h in NH_3-H_2-N_2 gas mixtures, with nitriding potentials indicated, or carburized at 507 °C (780 K) for 6 h in a CO-H_2-N_2 gas mixture. The lines are fitted by a Hill equation and show a sharper case-core transition for nitrided than for carburized material [42].

The expanded austenite zones are accompanied by huge compressive composition-induced residual stresses. Under practical conditions the nitrogen content should be kept below, say, 25 at.% N.

The transition from the hardened case to the unaffected austenite occurs within a narrow depth range, thereby enhancing the risk for pressing the hard shell into the soft underlying steel in case of a surface load. A remedy can be found in implementing a gradual transition from case to core by gaseous nitrocarburizing or by a two stage process, where nitriding is preceded by carburizing [42]. Accordingly, the hardened case consists of a zone of nitrogen-expanded austenite and a zone of carbon-expanded austenite underneath (Fig. 17). The interstitial atom content in carbon expanded austenite lies in the range from 0- 16 at.%C whereas for nitrogen-expanded austenite at least a nitrogen content corresponding to the Cr content is present [39]. Hence, carbon bridges the gap in interstitial atom content between unaffected austenite and nitrogen expanded austenite. Accordingly, smooth composition-depth, hardness-depth and residual stress-depth profiles can be tailored with a nitrocarburizing treatment.
For heavy loading of the surface the load bearing capacity of the austenite can be enhanced by high temperature solution nitriding preceding the low temperature hardening treatment [45].

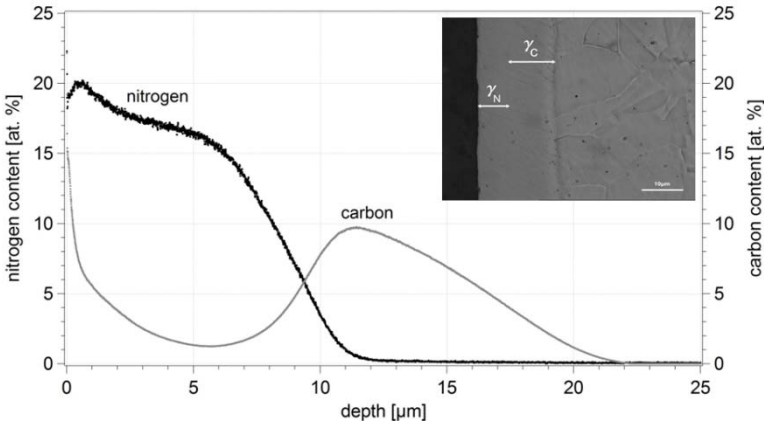

Fig.17: Nitrogen and carbon-depth profiles (GDOES) of AISI 316 nitrocarburized by linear heating from room temperature up to 475 °C (748 K) followed by immediate cooling in urea. Cross section shows subdivision in a nitrogen and carbon containing expanded austenite [45].

Future challenges

Even though a mature level of understanding thermodynamics, kinetics and microstructure development of nitriding and nitrocarburizing has been achieved, there are still many open questions to be answered. The thermodynamics of Fe-N phases appears to be well understood. On the other hand the thermodynamic understanding of Fe-N-C phases is still premature and the available (erroneous) data date back to the mid-sixties. For nitriding of iron the growth of the compound layer is satisfactorily described in terms diffusion controlled growth. Independent determination of diffusion coefficients of nitrogen in Fe-N phases by other experiments than layer growth experiments, appears necessary. Furthermore, the kinetics of the surface reactions, that play a decisive role on the actual surface concentration of nitrogen, are so far uninvestigated, despite the importance of these parameters for realistic modeling of the nitriding process. A basic understanding exists of the kinetics of nitrocarburizing and the influence on the microstructural evolution of the compound layer. However, no quantitative data for diffusion coefficients, surface reaction kinetics are available. A major challenge lies ahead to determine this data and to develop realistic models to mathematically describe compound layer growth.
The understanding of nitriding of special nitride forming steels (nitriding steels) appears well established. Also, a realistic mathematical description of the nitriding of Fe-M alloys is available. A full understanding of the role of carbon is so far not obtained, let alone a mathematical description.
Nitriding and nitrocarburizing of stainless steels is the research field that has experienced the fastest development in the last 10 years. Here, basic understanding of the mechanisms playing a decisive thermodynamic and kinetic role on the microstructure evolution. However, no realistic models to describe the thermodynamics of expanded austenite have so far been presented, which hinders a reliable mathematical description of the kinetics of growth of the diffusion zone (expanded austenite).

References

1. J. Slycke, L. Sproge, Surf. Eng., *5*, 1989, pp.125-140.
2. E.J. Mittemeijer, J. Slycke, Surf. Eng., *12*, 1996, pp.152-162.
3. H. J. Grabke, Mater. Sci. Forum, *154*, 1994, pp. 69-85.
4. K.-M. Winter, S. Hoja, H. Klümper-Westkamp, HTM J. Heat Treatm. Mat., 66, 2011,pp. 68-75.
5. H. Du, Somers, M.A.J., Ågren, J., Metall. Mater. Trans. A, *31A*, 2000, pp. 195-211.
6. E. Lehrer, Z. Elektrochem., 36, 1930, pp. 383-392.
7. B.J. Kooi, M.A.J. Somers, E.J. Mittemeijer, Metall. Mater. Trans. A, 27, pp. 1063-1071, 1996.
8. M.A.J. Somers, B.J. Kooi, L. Małdziński, E.J. Mittemeijer, A.A. van der Horst, A.M. van der Kraan, N.M. van der Pers, Acta Mater., 45, 1997, pp. 2013-2025.
9. E.J., Mittemeijer, M.A.J. Somers, *Surf. Eng.*, 13, 1997, pp. 483-497.
10. F.K. Naumann, G.L. Langenscheid, *Arch. Eisenhüttenwes.*, 36, 1965, pp. 677-682.
11. F.K. Naumann, G.L. Langenscheid, *Arch. Eisenhüttenwes.*, 36, 1965, pp. 583-590.
12. M.A.J. Somers, E.J. Mittemeijer, Härterei-Tech. Mitt., 47, 1992, pp.5-13.
13. M.A.J. Somers, Int. Heat Treatm. Surf. Eng., 5, 2011, pp.7- 16.
14. M.A.J. Somers, L. Małdziński, A.W.J. Gommers- unpublished work, Delft University of Technology, 1996.
15. M.A.J. Somers, E.J. Mittemeijer, Surf. Eng, 3, 1987, pp. 123-137.
16. S.S. Brenner, S.B. Goodman, Scripta Metall., 5, 1971, pp.865-870.
17. B. Mortimer, P. Grieveson, K.H. Jack, Scand. J. Metall., 1, 1972, pp. 203-209.
18. M. Pope, P. Grieveson, K.H. Jack, Scand. J. Metall., 2, 1973, pp. 29-34.
19. D.H. Kirkwood, O.E. Atasoy, S.R. Keown, Met. Sci., 8, 1974, pp.49-55.
20. K.H. Jack, Proc. Heat Treatment ´73, The Metals Society, Londen, 1975, pp. 39-50.
21. R. Wagner, S.S. Brenner, Acta Metall. 26, 1978, pp. 197-206.
22. P.M. Hekker, H.C.F. Rozendaal, E.J. Mittemeijer, J. Mater. Sci, 20, 1985, pp. 719-729
23. D.S. Rickerby, S. Henderson, A. Hendry, K.H. Jack, Acta Metall., 34, 1986, pp. 1687-1699.
24. C. Ginter, L. Torchane, J. Dulcy, M. Gantois, T. Turpin, A. Malchère, C. Esnouf, Metall. Ital., 98, 2006, pp. 29-35.
25. N.E. Vives Díaz, S.S. Hosmani, R.E. Schacherl, E.J. Mittemeijer, Acta Mater., 56, 2008, pp. 4137-4149
26. A.R.Clauss, E. Bischoff, S.S. Hosmani, R.E. Schacherl, E.J. Mittemeijer, Metall. Mater. Trans., 40A, 2009, pp. 1923-1934.
27. K.S. Jung, R.E. Schacherl, E. Bischoff, E.J. Mittemeijer, Surf. Coat. Tech. 204, 2010, pp. 1942
28. K.S. Jung, R.E. Schacherl, E.J. Mittemeijer, Phil. Mag., 91, 2011, pp. 2382-2403
29. K.S. Jung, S.R. Meka, R.E. Schacherl, E. Bischoff, E.J. Mittemeijer, Metall. Mater. Trans., 43A, 2012, pp. 934-944.
30. R.E. Schacherl, P.C.J. Graat, E.J. Mittemeijer, Metall. Mater. Trans.A, 35, 2004, 3387-3398.
31. S. S. Hosmani, R.E. Schacherl, E.J. Mittemeijer, Metall. Mater. Trans. A, 38, pp. 7-16.
32. B.J. Lightfoot, D.H. Jack, Proc. Heat Treatment ’73, The Metals Society, London, 1975, pp. 59-65.
33. Y. Sun, T. Bell, Mater. Sci. Eng.A, 224, 1997, pp.33-47.
34. P.C. van Wiggen, H.C.F. Rozendaal, E.J. Mittemeijer, J. Mater. Sci., 20, 1965, pp. 4561-4582.
35. S. Jegou, R. Kubler, L. Barrallier, M.A.J. Somers, HTM J. Heat Treatm. Mat., 66, 2011, pp. 135-142.
36. S. Jegou, Ph.D. Thesis, ENSAM ParisTech, 2009.
37. H. Oettel, G. Schreiber, Proc. Nitrieren und Nitrocarburieren, Eds. E.J. Mittemeijer, J. Grosch, AWT, Wiesbaden, 1991, pp. 139-151.
38. Z.L. Zhang and T. Bell, Surf. Eng., **1**, 1985, 131-136
39. T.L. Christiansen, M.A.J. Somers, Int. J. Mater. Res., 100, 2009, pp. 1361-1377.
40. H. Dong, Int. Mater. Rev., 55, 2010, pp. 65-98.
41. M.A.J. Somers, T. Christiansen, P. Møller, DK174707 B1 and EP 1521861 B1.
42. T. Christiansen and M.A.J. Somers, Surf. Eng., 21, 2005, pp. 445-455.
43. M.A.J. Somers. T. Christiansen, PCT: WO 2006136166_A1, 2006.
44. T.L. Christiansen, T.S. Hummelshøj, M.A.J. Somers, Surface Engineering, Vol. 27, No.8, 2011, pp.602-608.
45. T.L. Christiansen, T.S. Hummelshøj, M.A.J. Somers, PCT WO 2011 009463-A1.
46. T. Christiansen, M.A.J. Somers, Metall. Mater. Trans. A, 37, 2006, pp. 675-682.
47. J. Oddershede, T.L. Christiansen, K. Ståhl, M.A.J. Somers, 62, 2010, pp. 290-293.